PERGAMON

Journal of Structural Geology 23 (2001) 2011–2023

JOURNAL OF STRUCTURAL GEOLOGY

www.elsevier.com/locate/jstrugeo

# Two-dimensional geostatistical modeling and prediction of the fracture system in the Albala Granitic Pluton, SW Iberian Massif, Spain

J. Escuder Viruete[a,*], R. Carbonell[b], M.J. Jurado[b], D. Martí[b], A. Pérez-Estaún[b]

[a]*Depto. Petrología y Geoquímica, Universidad Complutense, E-28040 Madrid, Spain*
[b]*Inst. Ciencias de la Tèrra Jaume Almera-CSIC, Lluís Solé i Sabarís s/n, E-08028 Barcelona, Spain*

Received 2 August 2000; accepted 7 February 2001

**Abstract**

We use a fracture index distribution method of geostatistical modelling and prediction to characterize quantitatively the fracture system in two-dimensions (2D) in the Mina Ratones area, located in the Albalá Granitic Pluton (SW Iberian Massif). The fracture index (FI) is a quantitative estimate of the fracture density in discrete domains. To validate the results of geostatistical modeling a detailed structural map of the area was also made on a scale of 1:1000. The resulting grids, expressed as pixel-maps, describe the continuous value of the FI in 2D for the whole Mina Ratones area. Based on the modelled distribution of the FI and their correlation with mapped faults, we distinguish two structural domains in the studied area: elongated bands of fracture zones with high FI values and romboidal blocks located between them with low FI values. The separation between both domains is gradual. Though a threshold value of the FI that separate both structural domains is not clearly defined, the fracture zones generally present FI $> 1$ and the individualized blocks FI $< 0.50$. As a consequence, the obtained grid of the FI permits the quantitative structural classification of the granitic massif in 2D and understanding fault zone architecture in the Mina Ratones area. 

*Keywords*: Geostatistical modeling; Fracture system; Fracture index distribution method; Albalá Granitic Pluton; Iberian Variscan Massif

## 1. Introduction

A fault zone is typically a region that has a greater intensity of brittle deformation than the host rock. Commonly, faults can be divided into two distinct zones: the fault core, where most of the displacement is accommodated, and the damaged zone, which is mechanically related to the growth of the fault zone (Chester and Logan, 1987; Scholz and Anders, 1994). Fault core materials are usually composed of anastomosing slip surfaces, clay-rich gouge, cataclasite and fault breccias; damage zone structures are kinematically related fracture sets, small faults, veins and joints. The relative shapes and sizes of each of these structural components will vary from fault to fault and within a fault system and there may be more than one fault core or principal slip surface within a fault zone (Chester and Logan, 1987; Chester et al., 1993; Evans and Chester, 1995; Schulz and Evans, 1998, 2000).

Following the model of fault zone architecture of Caine et al. (1996), the fault core and damage zone are two distinct structural and hydrogeologic units that reflect the material properties and deformation conditions within a fault zone. This architecture controls the physical properties of fault zones as porosity, permeability, fluid flow and their mechanical behavior. Therefore, to determine the properties of a given fault zone, it is important to know the extention and spatial variability of the fault core and the damaged zone. However, insufficient data, particularly field-based data, are normally available to adequately characterize the architecture of fault zones found in areas where the outcrops are not continuous, nor homogeneously distributed.

An observed fact in many fault zones is that fracture density in the fault damage zone increases to the central fault core (Sibson, 1977; Hancock, 1985; Goddard and Evans, 1995; Schulz and Evans, 1998; Gillespie et al., 1993; Nedham et al., 1996). This fracture density can be quantitatively defined by a fracture index (FI), or number of structural discontinuities present by unit length of scanline in the outcrop (Narr and Suppe, 1991; Engelder et al., 1997). Based on the presence of this fracture density gradient perpendicular to a fault, FI estimates in discrete domains can be used to characterize fault zone architecture and their spatial variability. However, the estimates of the FI are also limited by the number and distribution of the outcrops and the areas between the outcrops are likely to be affected by a

* Corresponding author. Tel.: +34-91-394-4906; fax: +34-91-544-2535.
*E-mail address:* escuder@eucmax.sim.ucm.es (J. Escuder Viruete).

0191-8141/01/$ - see front matter 
PII: S0191-8141(01)00026-8

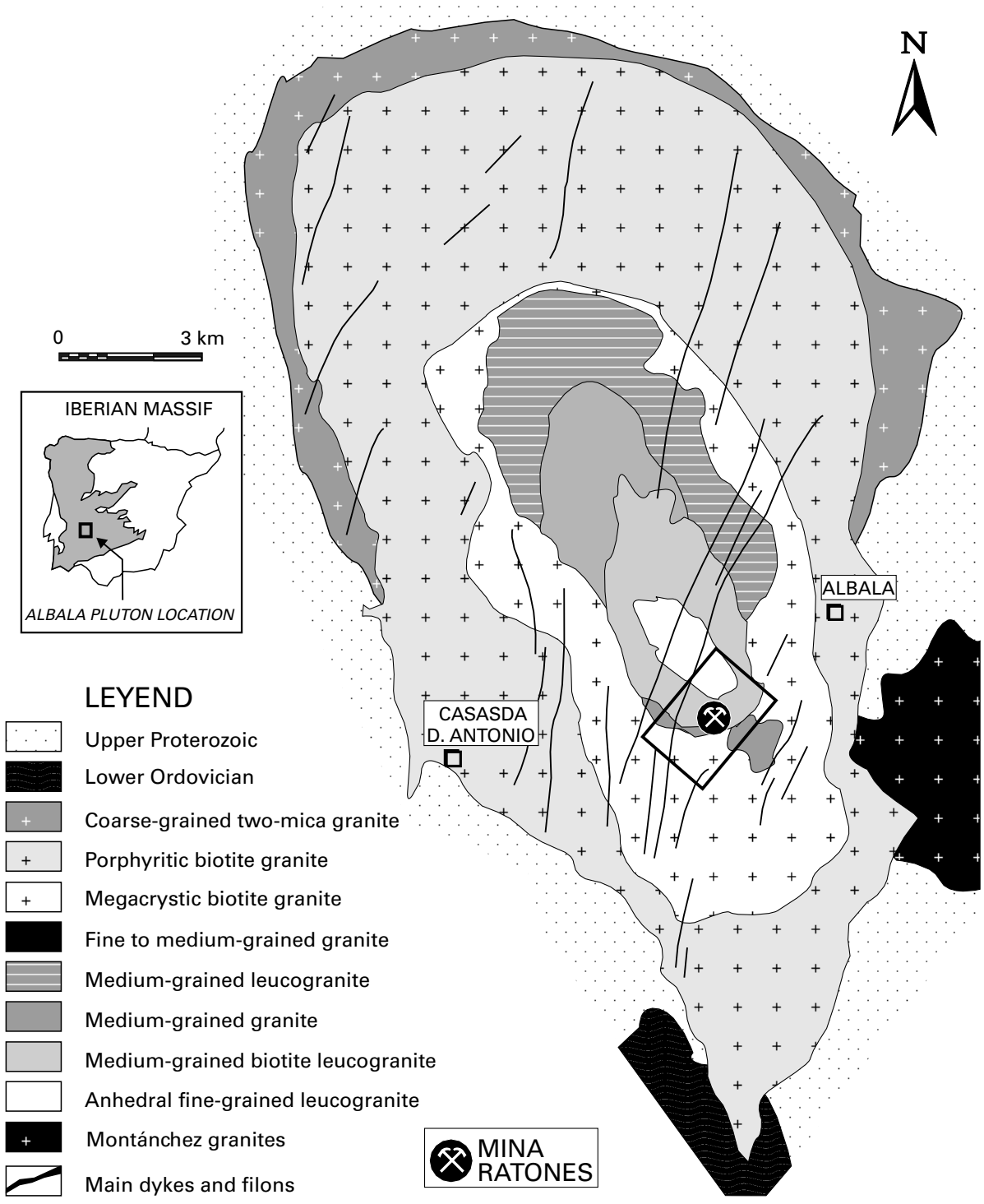


Fig. 1. Geological map of Albalá Granitic Pluton with location of the Mina Ratones area (Proyecto ZOA, 1996; Escuder Viruete and Pérez-Estaún, 1998).

greater fracture density than the outcrops themselves, particulary because of preferential erosion and weathering. A possible solution is to extrapolate the data of the FI in a given area using geostatistical techniques (Isaaks and Srivastava, 1989; Froidevaux, 1990; Cressie, 1991; Pannatier, 1996; Villaescusa and Brown, 1990; La Pointe and Barton, 1995).

The main objetive of this work is to test whether the FI distribution obtained from geostatistical modelling and prediction in the Mina Ratones area, Iberian Massif, characterizes quantitatively the fracture system in two-dimensions (2D). In this case, geostatistical data are FI values, estimates at known locations in the surface (geo-referenced), from a function that has a value at every

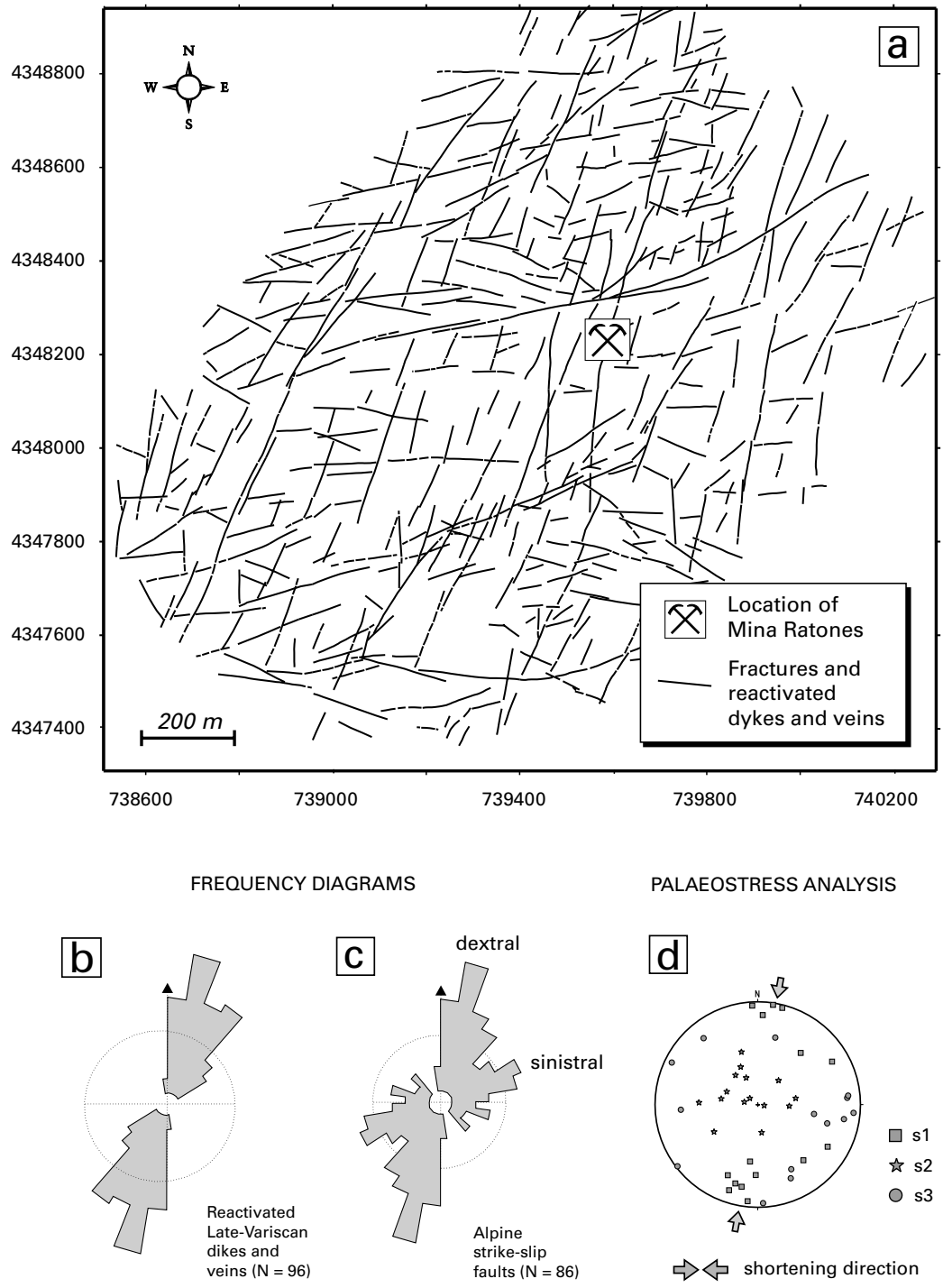


Fig. 2. (a) Structural map of brittle structures in the Mina Ratones area; (b) and (c) frequency diagrams of Late-Variscan and Alpine structures; (d) results of paleostress analysis carried out in Alpine strike-slip faults (Escuder Viruete, 1999).

location in a certain 2D domain. Geostatistical modelling of FI involves the estimation of the spatial correlation described in the sample variograms and fitting models to them (Englund and Sparks, 1991; Deutsch and Journel, 1992; Pebesma and Wesseling, 1998). Kriging is the geostatistical prediction method of the value of a spatially distributed variable from the adjacent values, considering the interdependence expressed in the model variogram (Pebesma and Wesseling, 1998). As an explicit assessment of the quality and limitations of geostatistical analysis, the results were compared with the fracture distribution obtained from the structural mapping of the Mina Ratones area on a scale of 1:1000. Furthermore, the range of the FI values that characterize the undeformed protolith, damaged zone and fault core in the Mina Ratones area are also determined.

## 2. Geological and structural setting

The Albalá Granitic Pluton is located in the southwest sector of the Iberian Massif (Central-Iberian Zone of Julivert et al. (1972)), which represents the westernmost segment of the European Variscan Belt (Pérez Estaún et al., 1991; Martínez Catalán et al., 1996). The granitoid is a concentric zoned body, elongated in a N–S direction, with porphyritic biotite granites in the rim and fine-grained two-mica leucogranites in the core (Fig. 1; Escuder Viruete, 1999). Major, trace and rare-elements suggest that magmatic rocks form a continous sequence ranging from granodiorites through granites, monzogranites to leucogranites (Gumiel and Campos, 1993). Rb–Sr whole rock ages indicate intrusion ages of $302 \pm 4$ Ma (Proyecto ZOA, 1996). Sn, W, P and U mineralization present in dykes are genetically related with the most differenciated leucogranitic hosted rocks (Reguilón, 1988; Reguilón et al., 1996). The origin of the uranium that gives rise to these mineralizations comes from the remobilization via fluid-phase of this element, present in the host leucogranite basically in the form of accessory uraninite. The mineralizing fluids filled fractures organized in a pattern, which is consistent with late-Variscan strike-slip tectonics (Castro, 1986; Sanderson et al., 1991; Proyecto ZOA, 1996). Mina Ratones is located in the central-southern sector of the Albalá Granitic Plutón (Fig. 1). Two main NNE–SSW oriented subvertical dykes (27 and 27′ Filons), with quartz, pichblenda, coffinite and black Fe–Mn oxides, were exploited between 1955 and 1974. The extracted mineral totaled 125,000 ton within the law of the 0.227% of uranium oxides (Arribas, 1962; Martínez and Ramírez, 1966).

During Alpine deformation, the pluton was affected by at least two phases of brittle deformation that cut ductile and ductile-brittle late-Variscan structures (Proyecto ZOA, 1996; Escuder Viruete and Pérez Estaún, 1998). Brittle structures in the Mina Ratones area are subvertical and can be geometrically grouped in two sets of different development: the sinistral NNE–SSW to ENE–WSW and the conjugate dextral N–S and NW–SE (Fig. 2a). Generally, the slip-vector associated with their planes have pitches of low-angle and, therefore, these structures can be classified as strike-slip faults. The kinematics of both fault sets suggest that $\sigma_1$ was subhorizontal and NNE-directed during a phase of brittle deformation, characterized by a wrench stress configuration. The NNE–SSW to NE–SW trend is also the direction of many late-Variscan subvertical dykes and faults, and these structures are frequently reactivated as strike-slip faults during this phase. The existence of mainly subvertical faults in the Mina Ratones area simplify the fracture modeling to a 2D problem.

At the outcrop scale, the strike-slip faults are defined by complex fault zones. These fault zones are characterized by abundant subparallel joints, shears and minor faults, with horizontal throw $<1$ m. The frequency diagrams of Fig. 2b and c shows the orientation of reactivated Late-Variscan dykes and Alpine strike-slip faults observed in the Mina Ratones area. These structures can be grouped in two main conjugated sets: NNE–SSW sinistral and ENE–WSW dextral, similar to sets observed at cartographic scale. The palaeostress analysis realized in some fault zones indicates that they were generated by a wrench stress configuration ($0.4 < R < 0.6$; $R = \sigma_2 - \sigma_3/\sigma_1 - \sigma_3$; Fig. 2d), characterized by a subhorizontal and NNE-directed trend of $\sigma_1$ and a subvertical orientation of $\sigma_3$ (Escuder Viruete, 1999). The thickness of individual fault zones can vary between 0.1 and 25 m, though narrow fault zones ($<0.5$ m) are more frequent. Some of the faults core rocks contain secondary U-mineralizations of gummite, autunite and torbernite, probably generated by U removilization in the fluid-phase through fault network, during the reactivation of late-Variscan dykes as Alpine strike-slip faults.

## 3. Geostatistical analysis

### 3.1. Variograms

Conventional statistics are based on the study of independent random variables that assume a null spatial continuity and they do not permit the extrapolation of the punctually measured values of a given property. Therefore, it is difficult to estimate the theoretical value of a property between the data, since all these intermediate points have the same general mean value. In geostatistics, however, it is assumed that the variables are continuous in space and their value is spatially correlated between adjacent points. The extension of the spatial correlation varies with the direction and is described in a variogram function (Isaaks and Srivastava, 1989; Goovarets, 1997). The spatial continuity can be used to estimate the values of the property in points, cells or blocks, in one-, two- or three-dimensions (1D, 2D or 3D).

The experimental variogram is calculated according to the following general equation (Deutsch and Journel, 1992; Pannatier, 1996):

$$\gamma(h) = [1/2N(h)]\Sigma[z_i - z_{i+h}]^2 \quad (1)$$

where $z_i$ is the measured value of the variable in the point $i$; $z_{i+h}$ is the measured value in the point $i + h$; $\gamma(h)$ is the semivariance in the interval of distance $h$; and $N(h)$ is the total number of $[z_i - z_{i+h}]$ pairs in the interval $h$. The calculation of $\gamma(h)$ is repeated for all intervals or ranges of $h$. If the first class size is say 100 m, then any pair of data points $[z_i - z_{i+h}]$, separated by a distance of 100 m are included in the computations for the first class size. Once this is completed, the calculations are repeated for the next class size and the process is repeated until some arbitrary stopping point is reached. The experimental variogram is obtained by plotting all the intervals of class $h$ versus the value of the semivariance $\gamma(h)$ calculated in each interval. If a spatial correlation exists between the data, typical

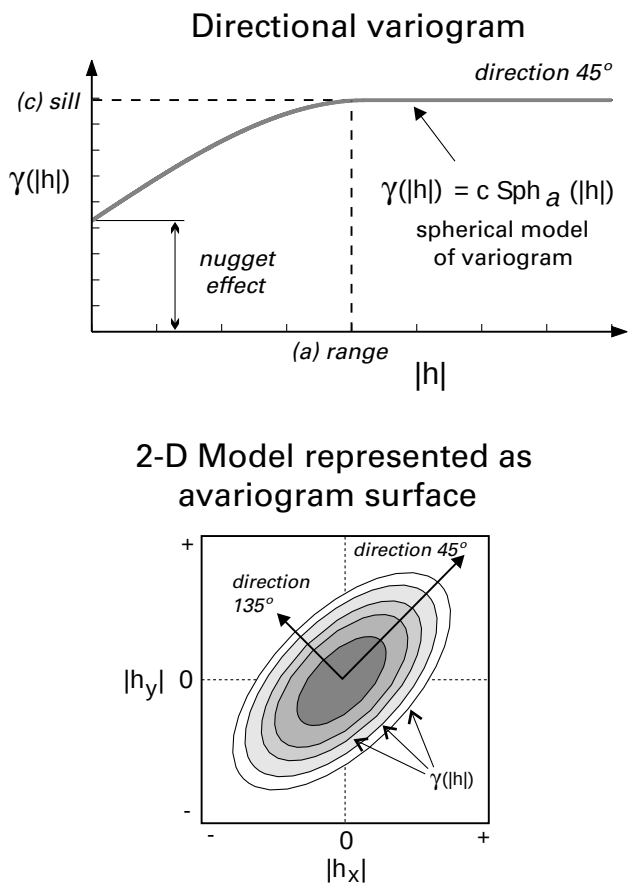


Fig. 3. A general 2D spherical model viewed in a specific direction (45°), or directional variogram, and its synthetic representation as a variogram surface.

variograms are convex curves where it is possible to extract several parameters that define the spatial continuity model of the property (Fig. 3), following the methodology described below.

### 3.2. Geostatistical methodology and data collection

Typically, geostatistical analyses have several steps (Cressie, 1991; Pannatier, 1996). In the present study, the first step consisted of building a geo-referenced data-base of FI, as a measure of the fracture density in a discrete domain. Regularly spaced high quality exposures, where rocks are cut by one or several joint and fault sets, were selected in the study area (Fig. 4). At each station, fracture spacing data were collected by placing a scanline of at least 30 m perpendicular to the strike of the main differently oriented fracture sets. The intersection of the joints with the scanline was recorded and, in the case of faults, throw, dip-direction, dip-angle and vector of movement for the geometric and kinematic analysis. Obtained values of FI were stored in ASCII files of similar format to *Geo-Eas* and *GSLIB* data-files (Englund and Sparks, 1991; Deutsch and Journel, 1992).

The second step was to obtain the experimental variogram surface, where it was possible to detect directional anisotropies in the pattern of spatial continuity (Isaaks and Srivastava, 1989; Pannatier, 1996). Following the observed main spatial directions in this surface, directional variograms were calculated. In the case of Mina Ratones, these main spatial continuity directions of FI should logically coincide with the main trends of small-scale fractures and mapped faults. Through an iterative process, a theoretical variogram model was adjusted to the directional variograms. The geometry of this variogram defines the parameters of the geostatistical model.

The third step was introducing the nested model parameters of spatial continuity as an interpolation procedure (kriging) between the measured data of the FI. As a result, the total set of discrete values of the FI, measured and calculated, form mesh points or a grid that describes the continuous value of the fracture property in 2D. The grids can be edited as maps of various types that constitute the optimum geostatistical representation of the property.

However, the values of the FI obtained by kriging normally have a lower range of variation than the estimated values of FI in the stations. That is, the predicted field is smoother than the field from which the observations were obtained (Pebesma and Wesseling, 1998). As will be seen below, in the most fractured zones this causes the prediction of a smaller value for the FI than the measured value. Residual maps that describe the differences between the measured and estimated values of the FI provide a method that will permit us to know how much kriging reproduces reality in terms of FI variability and evaluate the quality of the kriging.

### 3.3. Statistics of the fracture index

For a total of 115 stations, measured minimum and maximum values of FI are 0.18 and 3.2, respectively (Table 1). The resulting mean value for the FI is 0.798, with a standard deviation of 0.498. The frequency distribution is clearly unimodal (Fig. 5), with a negative asymmetry and 0.46 as mode value. Therefore, the distribution is of log-normal type, with 1.55 of skewness and 3.97 of kurtosis. In Table 1, the statistical parameters of the population resulting from the log-normal transformation of FI data, or *LogFI* variable, are also summarized. This transformation of data is necessary to make the distribution more symmetrical and to remove the trend in variance (Journel, 1989). The resulting distribution tends to be bimodal and, eliminating the log-normal transformation, the more frequent values of the FI are 0.18 and 1.66 (Fig. 5; Table 1).

### 3.4. Fracture index variogram surface

Before a variographic study of the FI is performed, it is necessary to calculate all the possible $[z_i - z_{i+h}]$ pairs and order them according to the distance $h$ (Froidevaux, 1990). For a total of 6105 pairs, the variogram surface was built for

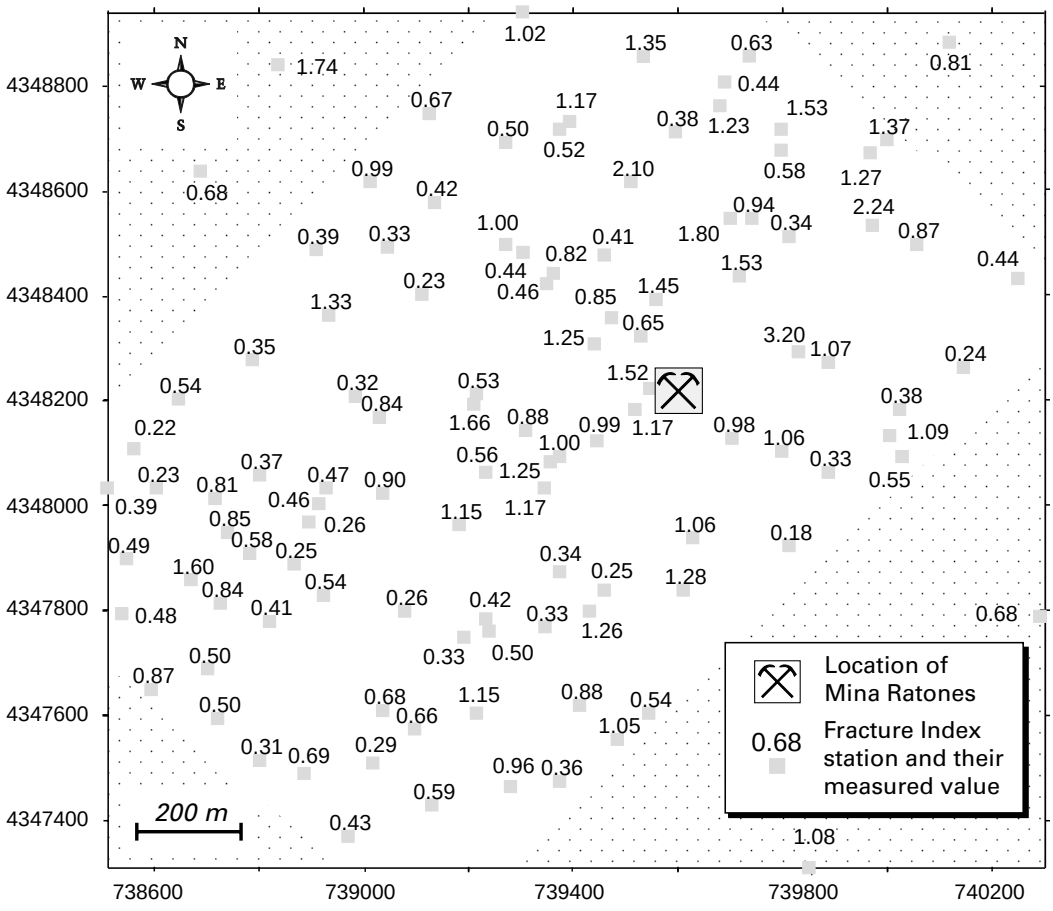


Fig. 4. Map showing the location of stations of fracture index (FI) measure in the Mina Ratones area. Location shown by national grid references (UTM) of N–S and E–W frame lines. Sectors of poor or no data within outer map boundary are stippled.

the *LogIF* variable with *Vario2D* routine (Pannatier, 1996), taking six lags of 160 m along *X*-direction (east) and *Y*-direction (north), and visualized in the form of a pixel-map (Fig. 6). Each pixel of the surface represents a measure of the spatial continuity, which is a function of $h$ or their components $h_x - h_y$. The resulting variogram surface shows that the FI presents a maximum of continuity along the 050° and 075° compass directions and a minimum following the 140° direction. As was expected for the Mina Ratones area, the direction 075° of maximum continuity of the FI coincide with the ENE–WSW fracture set, frequent at all scales. However, the main NNE–SSW fracture set appears defined by relatively high values of spatial continuity, but not defining of a maximum in the surface. The maximum of continuity obtained along the direction 050° represents the mean trend between the NNE–SSW and ENE–WSW fault sets, which define a romboidal pattern in the structural map of Fig. 2.

Table 1
Summary statistics of fracture index (FI) data for the Mina Ratones area

| | Non-transformed | Transformed |
|---|---|---|
| Mean | 0.798 | − 0.403 |
| Std. deviation | 0.498 | 0.603 |
| Sample variance | 0.248 | 0.364 |
| Minimum value | 0.180 | − 1.715 |
| Maximum value | 3.200 | 1.163 |
| Skewness (se) | 1.55 (0.23) | 0.02 (0.23) |
| Kurtosis (se) | 3.97 (0.46) | − 0.73 (0.46) |

### 3.5. Fracture index directional variograms

The FI directional variograms of Fig. 7 were obtained from four sections of the variogram surface, along the directions 050°, 075°, 100° and 140°. These directional variograms were built with *Geo-EAS* (Englund and Sparks, 1991) and *Variowin* geostatistical software (Pannatier, 1996). *Variowin* software possess graphic capacities to identify pairs that have a strong influence on the measure of the spatial continuity. In the variograms, the distance $h$ and the number of lags are 200 m and eight, respectively, covering a distance of 1600 m for a tolerance angle of 30°.

### 3.6. Two-dimensional fracture index modeling

The directional variograms can be used to adjust a theoretical variogram model that describes the 2D spatial continuity of FI. Being the crucial part of most geostatistical

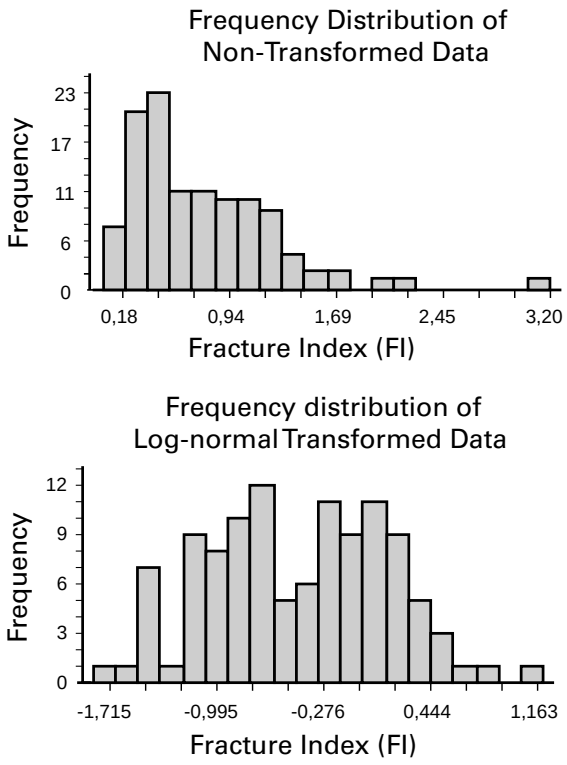


Fig. 5. Statistic of fracture index (FI) data for the Mina Ratones area. *LogFI* variable is the log-normal transformation of FI in order to better normalize the skewed frequency distribution prior to geostatistical analysis.

studies, variogram modelling should be done interactively (Deutsch and Journel, 1992). For this analysis *Model* (Pannatier, 1996) and *GSTAT* (Pebesma and Wesseling, 1998) were used. Both programs provide an interactive user interface for graphical display and adjusts the variogram model to the sample variograms simultaneously along several directions.

In Fig. 7, the fitted model variogram appears as a convex curve defined by the following expression:

$$\gamma(h) = 0.0343 + \{0.0378 \times Sph(h)\} \quad (2)$$

where $Sph(h) = \{1.5(h/913.973) - 0.5(h/913.973)^3\}$ if $|h| \leq 913.973$. The resulting nested model of spatial continuity of FI is spherical and their parameters defined by nugget = 0.0343, range = 913.973 and sill = 0.038. The structure has a direction of 050° and an anisotropy of 0.7, defined by the maximum range/minimum range ratio. The covariance obtained for the variable *LogIF* is $6.819 \times 10^{-2}$. The measure of a good adjustment between sample variograms and the variogram model is indicated by the low values of the standardized parameter IGF = $2.269 \times 10^{-2}$ (Indicative Goodness of Fit; Pannatier, 1996). The IGF parameter is a number without units and a value close to zero indicates a good fit. In summary, the obtained 2D nested model of spatial continuity of the FI is the sum of an isotropic nugget effect and a simple anisotropic structure of spherical type.

The variogram surface plot in Fig. 8 is a representation of the 2D model of spatial continuity of the FI in the Mina Ratones area. The selected lag in the *X* and *Y* directions is 25 m with 500 m as the upper and lower limits. The maximum and minimum continuity directions of *LogFI* are variable, indicated by the main axes of the ellipse, and coincide with the main directions of anisotropy observed in the experimental variogram surface (Fig. 6), but they do not reproduce the oscillations of the variable about the sill, visible in the 100° and 140° directional variograms (Fig. 7).

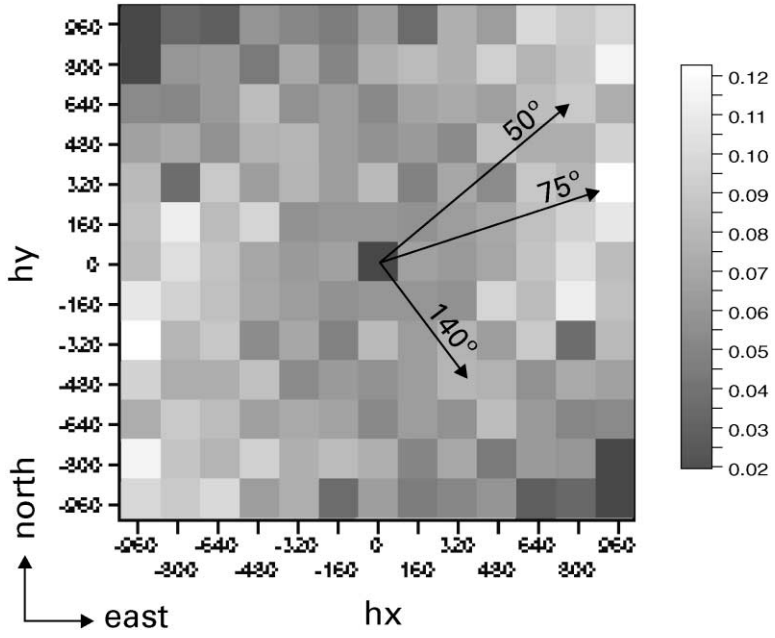


Fig. 6. Variogram surface of fracture index (FI) for the Mina Ratones area. The variogram surface shows that the variable *LogFI* has a maximum continuity in the directions of 50° and 75°, and a minimum continuity in the direction of 140°.

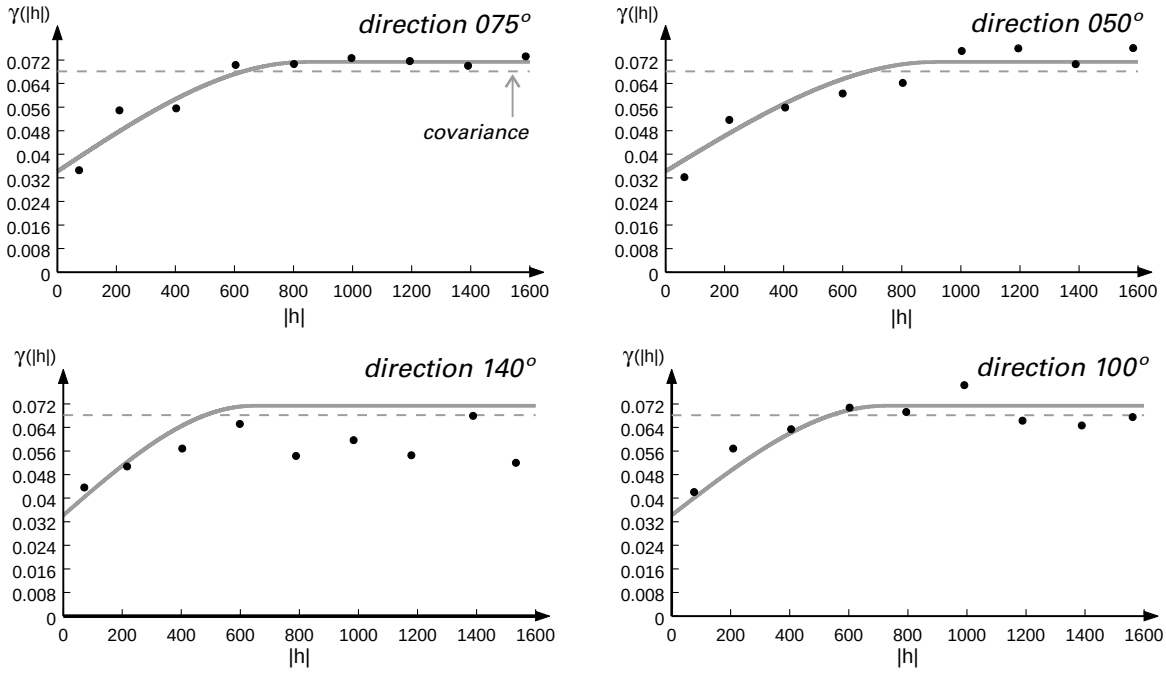


Fig. 7. Experimental directional variograms (*LogFI* variable) calculated along the directions of maximum and minimum continuity identified on the variogram surface of Fig. 6. The black points are the $\gamma|h|$ values calculated each lag of 200 m. The convex gray curve is the fitted model variogram. The horizontal black line is the covariance obtained for the variable *LogFI* ($6.819 \times 10^{-2}$). The obtained 2D nested model of spatial continuity is the sum of an isotropic nugget effect and a simple anisotropic structure of spherical type (see text for a explanation).

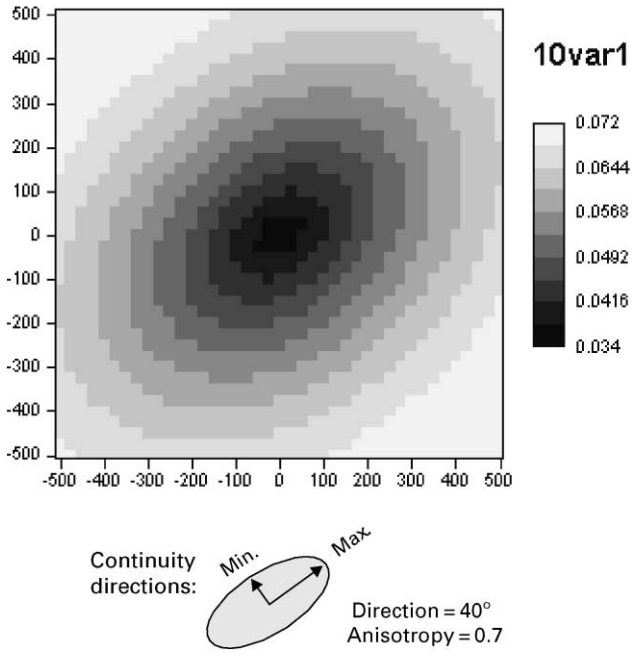


Fig. 8. Modeled variogram surface of fracture index (FI) in the Mina Ratones area. The 2D nested model of spatial continuity reproduces the main directions of anisotropy observed on the experimental variogram surface (Fig. 6), but it does not reproduce the 'hole effects' (Pannatier, 1996) visible in the 130° and 170° directions.

### 3.7. Two-dimensional fracture index prediction

With the parameters of the spatial continuity model previously defined, ordinary kriging was used for FI prediction, due to the heterogeneous FI data distribution in the Mina Ratones area. *KRIGE2* routine (Froidevaux, 1990) and *GSTAT* software (Pebesma and Wesseling, 1998) were used for kriging with similar results. Output files are ASCII grids or simplified *GeoEAS* format files (Englund and Sparks, 1991). The obtained results are shown in Figs. 9–12.

Fig. 9 is a pixel map built from the grid with the FI values estimated by kriging. The grid is defined by cells disposed to regular intervals, filling a rectangle whose sides are oriented parallel to the *X*-direction (east) and *Y*-direction (north). The number of cells is $50 \times 46$ ($X \times Y$) and the dimensions of a cell are $39 \times 32$ m$^2$, similar in size to that of the scanlines used for the determination of FI. The large rectangle indicates the mapped area next to Mina Ratones, where more FI data were estimated; outside of it the predictions of the FI are less rigorous.

In the figure, gray and white tones correspond to zones with low and high FI, respectively. These zones are elongated following the NNE–SSW to NE–SW and ENE–WSW directions, which coincide with the trend of the main mapped faults. In the SE sector of Mina Ratones, the FI presents values of near 0.25 and individualizes a NE-striking zone characterized by a low fracture density. To the W and NW, an elongate transitional zone appear toward a more fractured domain, defined by FI values between 1.35

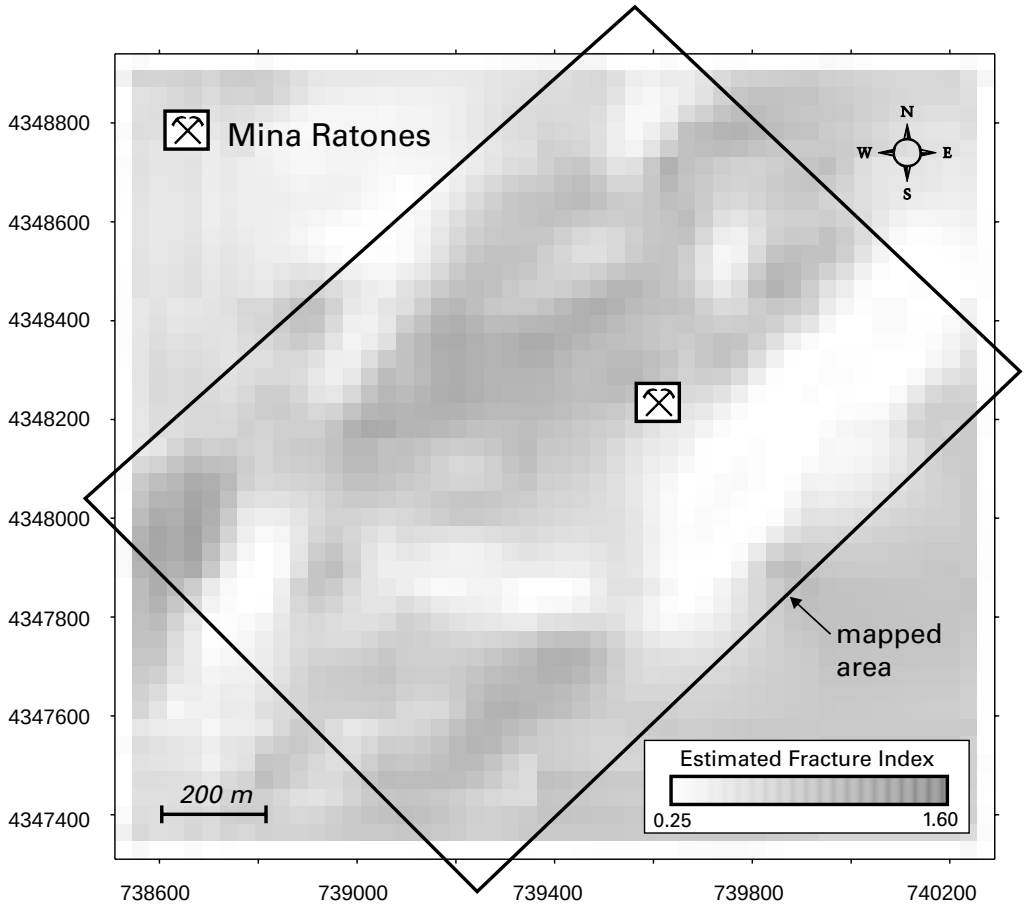


Fig. 9. Pixel-map built from the grid-file of the fracture index (FI) estimated by kriging in the Mina Ratones area.

and 1.6. A fact observed in the field is that, in the damage zone of the main faults, the measured value of the FI increase in a normal direction toward the fault core. This fault density gradient adjacent to major strike-slip faults (and related brittle strain) has been also previously recognized by Little (1996) and Caine et al. (1996). In this sense, it is interesting to compare the distribution of FI values predicted by kriging in 2D with the traces of main mapped faults.

Fig. 10 results from superimposing the trace of all mapped dykes and fractures in the Mina Ratones area onto the FI grid. As observed in the figure, gray tone bands of greater FI and the zones with a high fracture density, or with faults of greater length, are well correlated. This is especially valid along a ENE–WSW directed band, located in the north sector of the Mina Ratones, which coincides with the trace of one of the main mapped structures, the North Fault. Framed by subvertical faults of great length and characterized by a low cartographic fracture density, a sector with white tones of low FI is defined to the SE sector of the mine. Therefore, the obtained distribution of the FI and their correlation with mapped faults permits us to distinguish two structural domains in the studied area: elongated bands of fracture zones and romboidal blocks located between them. As a consequence, the construction of grids of the FI permits the quantitative structural classification of the granitic massif in 2D. Both structural domains most probably correspond with the protolith and the damage zone/fault core in the model for fault zone architecture of Caine et al. (1996). Though a threshold value of the FI that separates both structural domains is not clearly observed, $FI > 1$ in the fracture zones and $FI < 0.50$ in the individualized blocks. If we admitted that the two modes obtained in the frequency distribution of *LogFI* data represent both structural domains (Fig. 5), the intermediate values establish a threshold of approximately 0.45.

### *3.8. Relationships between fracture index distribution and transmissive faults*

Fault zone architecture and related permeability structures form primary controls on fluid flow in brittle fault zones. Hydraulic tests, geophysical measurements and petrophysical sampling in several drilled boreholes indicates that the granitic rocks of Mina Ratones have a very low primary porosity, with water located in the pores of the fault rocks associated with the fractures (Gómez et al., 1998). For this reason, it is interesting to relate the architecture and permeability structure of the faults with the distribution of the FI in the Mina Ratones area. Fault zone architecture and permeability structure are characterized by

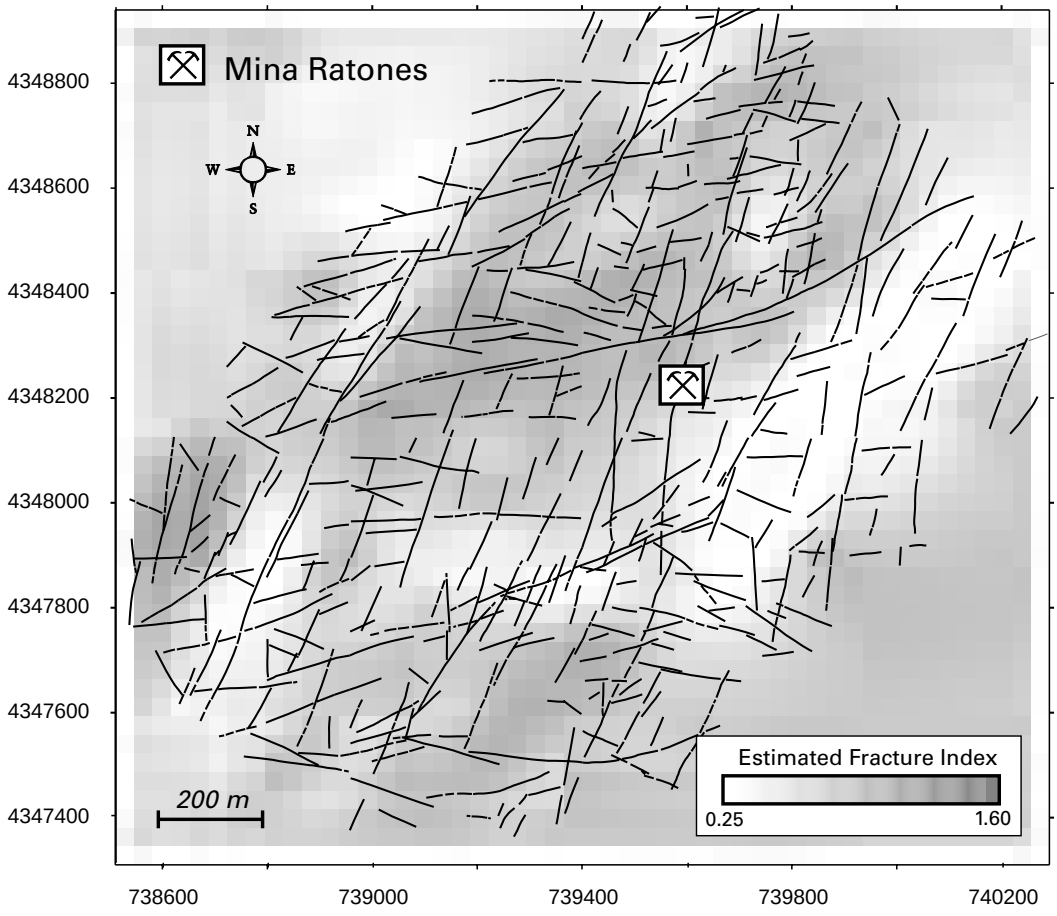


Fig. 10. Relationships between mapped faults and the grid (pixel-map) of fracture index (FI) in the Mina Ratones area (see text for an explanation).

plotting values of $F_a$ against total fault zone width, where $F_a$ = damage zone width/total fault zone width (Caine et al., 1996). Fig. 11 shows values of $F_a$ plotted for several different fault zones with a high transmissivity in the Mina Ratones area, defined from controlled pumping tests (Gómez et al., 1998). The data shown suggest that these fault zones are damage zone dominated, with $F_a$ values between 0.79 and 0.93. $F_a$ values near to one indicate that the fault core is absent or poorly developed and the presence of a higher permeability damage zone causes the fault zone to act as a conduit for flow. This is consistent with well-developed discrete slip surfaces and associated fracture networks in the broad damage zone of these faults, which reflect a distributed strain and cause a conduit-type permeability structure.

Fig. 12 shows the relationships between the grid of the FI and the high transmissive faults in the Mina Ratones area. As is observed in the figure, a good correlation exists between elongated and broad gray zones, indicative of well-developed damage zones with high values of the FI, and traces of the more transmissive faults. For example, the subvertical North Fault is well defined by a 100–150 m width band where FI $> 1$ and the pair of 27 and 27′ dykes are included in a NNE–SSW directed band with high values of FI. However, the porphyritic granite dyke only presents a high IF in the intersection with the North Fault, a fact observed in the field, and the South Fault does not coincide clearly with a high density fracture band, which is due, in this case, to a poorly developed damage zone of 5–20 m. These relationships suggest that the damage zone can be defined by the spatial distribution of the FI. In the Mina Ratones area, well-developed damage zones with a permeability structure of distributed conduit are expressed by broad bands of high values of FI, generally greater than 1.35. Therefore, the geostatistical modelling of FI provides a predictive tool for better understanding fault zone architecture and their permeability structure.

### *3.9. Uncertainties in the estimation of the fracture index*

The uncertainties in the estimation of the FI were evaluated comparing the values measured in the stations with those estimates by kriging. Generally, a close correspondence existed between the zones with a predicted high FI with the greater measured values of the FI. However, there locally exists high values of the measured FI in zones with a low predicted index, and vice versa. This is due to the smoothing effect in the value of the FI that

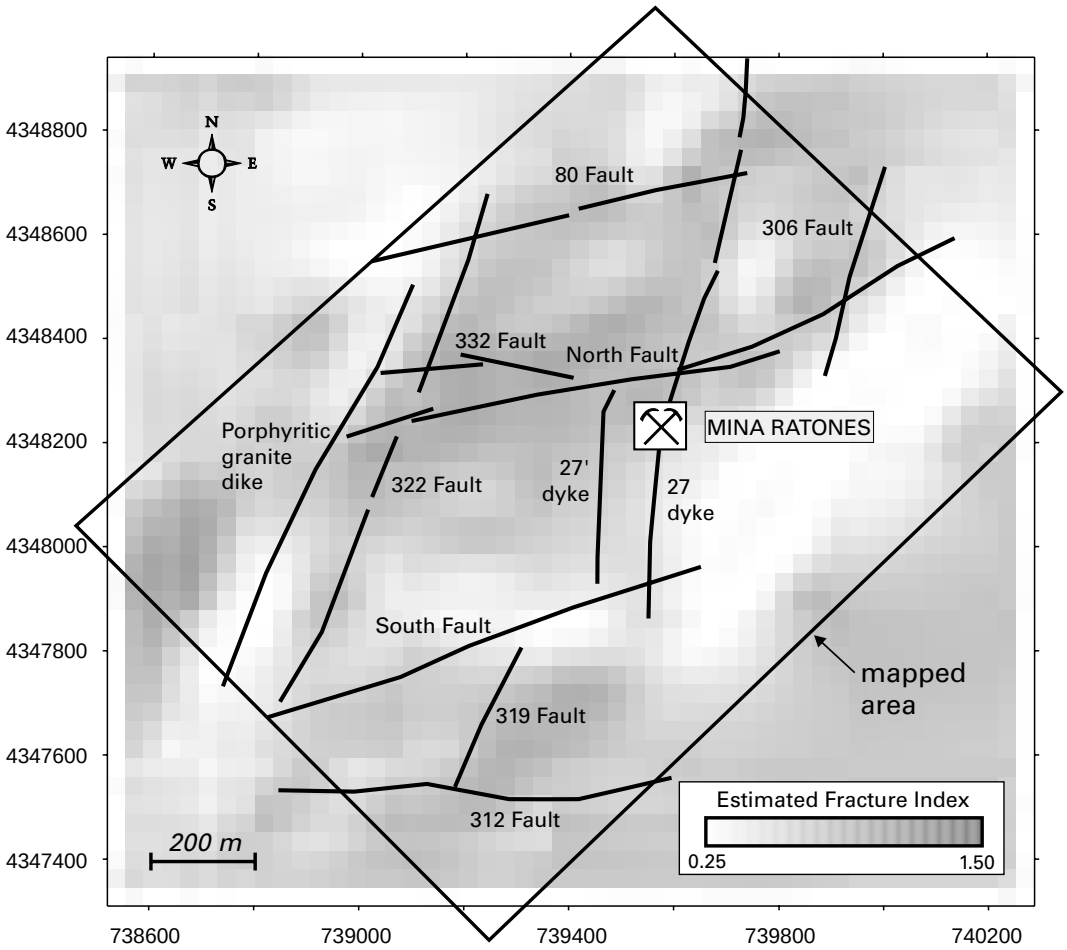


Fig. 11. Relationships between the grid (pixel-map) of fracture index (FI) and faults with a high transmissivity in the Mina Ratones area. Two structural domains in base to the index values are defined: fracture zones (FI > 1, gray tones) and romboidal blocks located between them (FI < 0.5, white tones).

originates the process of kriging, where high original values tend to be underestimated and low values overestimated, with a smaller range of predicted FI than the original values (Pebesma and Wesseling, 1998).

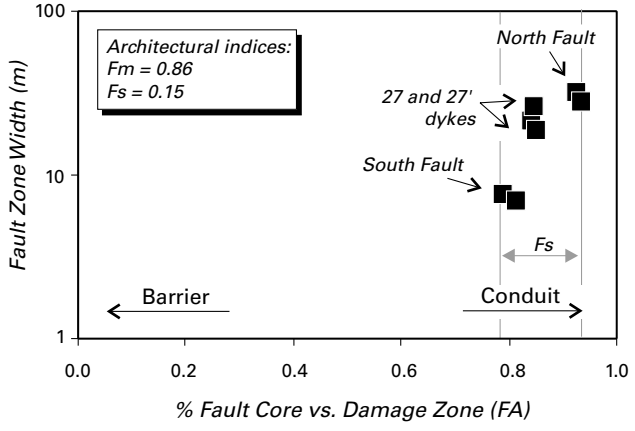


Fig. 12. Fault zone architecture and permeability structure plots of Caine et al. (1996). Data from high transmissive faults of the Mina Ratones area. Architectural indices: $F_a$ = damage zone width/total fault zone width; $F_m$ = mean of $F_a$ values for a zone; $F_s = (F_a)_{max} - (F_a)_{min}$.

The residuals of the FI in the Mina Ratones area are represented in the pixel-map of Fig. 13. They result from the difference (in absolute value) between the values of FI measured and estimated by kriging in the cell where the station is located. The residuals range between 0.05 and 0.85, and were linearly interpolated through a simple method of triangulation to generate the grid. Generally, the greater residuals (white tones) are located in the zones with a predicted high FI and the smaller residuals (gray tones) in those of low FI. A similar correspondence is obtained by superimposing upon the pixel-map the trace of the main mapped faults (Fig. 13). The greater residuals are spatially associated with the main faults and the smaller residuals with the romboidal blocks characterized by a low fracture density. These relationships indicate that the uncertainities in the estimation of the FI would be greater for the fracture zones than in the blocks located between them.

## 4. Conclusions

The main objective of this work is to test whether the FI

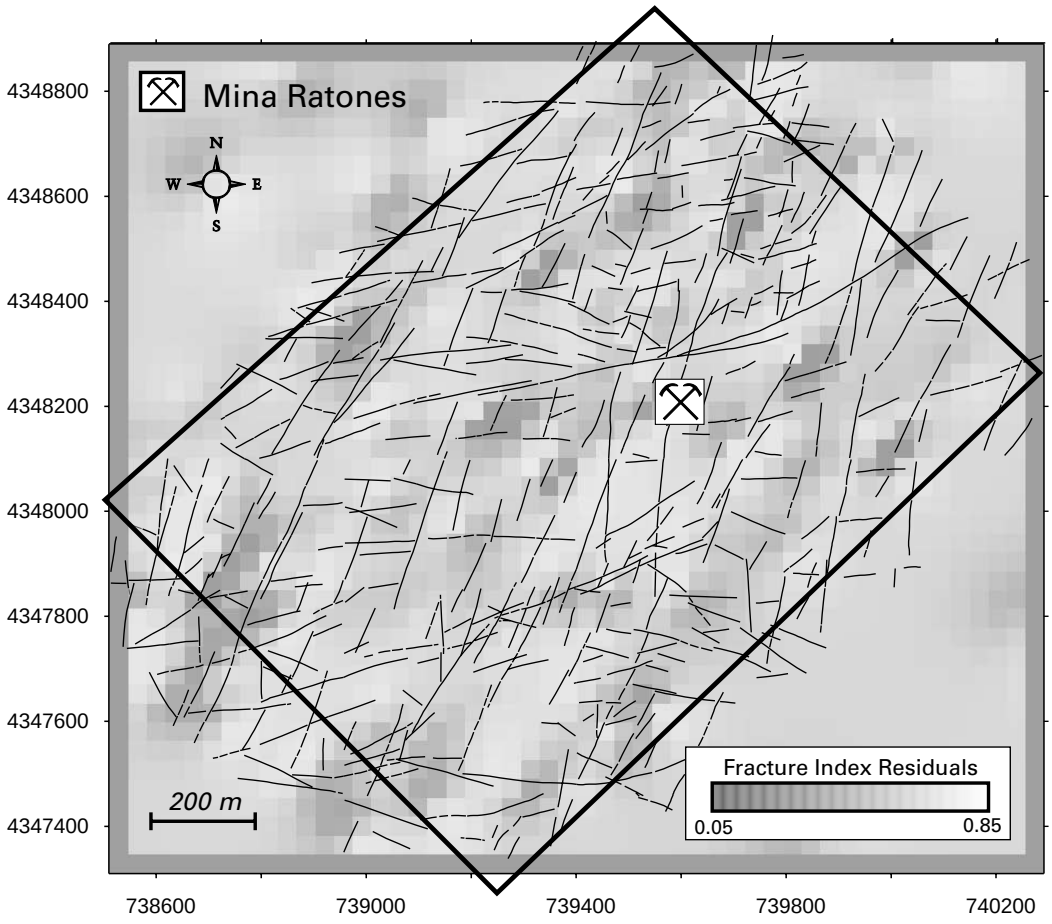


Fig. 13. Pixel-map built from the grid-file that stores the residuals of the fracture index (FI) in the Mina Ratones area. These residuals are the difference, in absolute value, between the value of the index measured in the stations and the estimate by kriging (see text for a explanation).

distribution obtained from geostatistical modelling and prediction characterizes quantitatively the fracture system of the Mina Ratones area in 2D. The methodology consists of: (1) building a geo-referenced database of the FI, (2) calculating directional sample variograms parallel to the directions of greater spatial continuity, generally coincident with the trend of the main mapped faults, (3) from an interactive process, fitting a theoretical model of variograms to the sample variograms, thus obtaining the model parameters of the spatial continuity, and (4) introducing a nested model to interpolate (krige) between the original data of the FI measured in the stations. The resulting grids describe the continuous value of the FI in 2D for the whole Mina Ratones area.

The grids, expressed as pixel-maps, show zones with high and low values of FI. The obtained distribution of the FI and their correlation with mapped faults permits us to distinguish two structural domains in the studied area: elongated bands of fracture zones and romboidal blocks located between them. Both structural domains most probably correspond with the protolith and the damage zone/fault core in the model for fault zone architecture of Caine et al. (1996). Therefore, the construction of grids of the FI in areas affected by strike-slip brittle tectonics, as Mina Ratones, permits the quantitative structural classification of the rock massif.

This classification permits volumetric calculations in the rock massif and has a predictive character. For example, considering a vertical dimension (depth) for the cells of 100 m, the volume of rock with $0.01 < \mathrm{FI} < 0.6$ is of 2,855,486 $m^3$ in the Mina Ratones area. This volume is calculated by adding the volume of all cells of the index within the specified range. The existing correlation between FI and main mapped faults can be applied to the classification of the rock massif, even in zones with minor outcrops and where the main faults may not have been detected. In the Mina Ratones area, well developed damage zones with a permeability structure of distributed conduit ($F_a$ values of 0.79–0.93) are expressed by broad bands of high values of FI (in our case $F > 1.35$). In this sense, the geostatistical modelling of FI also provides a predictive tool for better understanding fault zone architecture and their permeability structure. Finally, further development of geostatistical methods exposed in this study will include the modelling and prediction of fracturation in 3D, taking into account surface and borehole log data of FI.

## Acknowledgements

This work represents part of the structural results of a multi-disciplinary project carried out for the environmental restoration of old uranium mines supported by ENRESA. Discussions with many colleagues of the CIEMAT, Universidad Politécnica de Cataluña and AITEMIN have contributed greatly to our understanding of faults in Mina Ratones. This manuscript benefitted from useful reviews by J.P. Evans, O. Roleau and an anonymous reviewer.

## References

Arribas, A., 1962. Mineralogía y Metalogía de los yacimientos españoles del uranio: Los Ratones, Albalá (Cáceres). Estudios Geológicos. Vol. XVIII. Madrid.

Caine, J.S., Evans, J.P., Forster, C.B., 1996. Fault zone architecture and permeability structure. Geology 24, 1025–1028.

Castro, A., 1986. Structural pattern and ascent model in the Central Extremadura Batholith, Hercynian Belt, Spain. Journal of Structural Geology. 8, 635–645.

Chester, F.M., Logan, J.M., 1987. Composite planar fabric of gouge from the Punchbowl Fault, California. Journal of Structural Geology. 9, 621–634.

Chester, F.M., Evans, J.P., Biegel, R.L., 1993. Internal structure and weakening mechanisms of the San Andreas fault. Journal of Geophysical Research. 98, 771–786.

Cressie, N., 1991. Statistics for Spatial Data. John Wiley & Sons, New York.

Deutsch, C.V., Journel, A.G., 1992. GSLIB: Geostatistical Software Library and User's Guide. Oxford University Press, New York.

Engelder, T., Gross, M.R., Pinkerton, P., 1997. Joint development in clastic rocks of the Elk Basin anticline, Montana, Wyoming. In: Hoak, T., Klawitter, A., Blomquist, P. (Eds.). An Analysis of Fracture Spacing versus Bed Thickness in a Basement-involved Laramide Structure. , pp. 1–18 Rocky Mountain Association Geol. 1997 Guidebook, Denver.

Englund, E., Sparks, A., 1991. Geo-EAS 1.2.1 User's Guide. EPA Report 600/8-91/008 EPA-EMSL, Las Vegas, Nevada.

Escuder Viruete, J., 1999. Evolución del campo de esfuerzos alpino y cinemática de las fallas en el entorno de la Mina Ratones, Plutón Granitico de Albalá, Extremadura Central. XV Reunión. Geología del Oeste Peninsular. Diputación de Badajoz, pp. 109–114.

Escuder Viruete, J., Pérez Estaún, A., 1998. Estudios Geológico-Estructurales y Geofísicos en la Mina Ratones: Estructura. Informe de Avance ENRESA (10-CJA-IA-05). Madrid, 33pp.

Evans, J.P., Chester, F.M., 1995. Fluid–rock interaction in faults of the San Andreas system: inference from San Gabriel fault-rock geochemistry and microstructures. Jornal of Geophysical Research. 100, 13007–13020.

Froidevaux, R., 1990. Geostatistical Toolbox, version 1.30, FSS International, Chemin de Drize 10, 1256 Troinex, Switzerland.

Gillespie, P.A., Howard, C.B., Walsh, J.J., Wartterson, J., 1993. Measurement and characterization of spatial distributions of fractures. Tectonophysics 226, 113–141.

Goddard, J., Evans, J.P., 1995. Chemical changes and fluid–rock interaction in faults of crystalline thrust sheets, northwestern Wyoming, USA. Journal of Structural Geology 17, 533–547.

Gómez, P., Ruiz, B., Floria, E., Garralón, A., García. M., 1998. Caracterización hidroquímica de las aguas subterréneas en la Mina Ratones: (Parte I) Metodologías utilizadas para el muestreo de aguas y su caracterización. Informe de Avance, ENRESA. Madrid, 138pp.

Goovarets, P., 1997. Geostatistics for Natural Resources Evaluation. Oxford University Press, New York.

Gumiel, P., Campos, R., 1993. Contribución al conocimiento geológico y geoquímico de los granitos de Albalá y Montánchez (Extremadura Central) y su relación con las mineralizaciones de estaño y wolframio. Geogaceta 13, 57–61.

Hancock, P.L., 1985. Brittle microtectonics: principes and practice. Journal of Structural Geology. 7, 437–457.

Isaaks, E., Srivastava, R.M., 1989. An Introduction to Applied Geostatistics. Oxford University Press, New York.

Journel, A.G., 1989. Fundamentals of Geostatistics in Five Lessons. Short Course in Geology, Vol. 8. Americal Geophysical Union, Washington.

Julivert, M., Fontbote, J.M., Ribeiro, A., Conde, L., 1972. Mapa Tectónico de la Península Ibérica y Baleares. E. 1:1,000,000. IGME, Madrid.

La Pointe, P.R., Barton, C.C., 1995. Creating reservoir simulations with fractal characteristics. In: Barton, C.C., La Pointe, P. (Eds.). Fractal in Petroleum Geology and Earth Processes. Plenum Press, New York, pp. 263–278.

Little, T.A., 1996. Faulting-related displacement gradients and strain adjacent to the Aware strike-slip fault in New Zealand. Journal of Structural Geology. 18, 321–340.

Martínez, A., Ramírez, E., 1966. El yacimiento uranífero de Los Ratones, Albalá (Cáceres). Boletín Geológico y Minero 41, 1–28.

Martínez Catalán, J.R., Arenas, R., Díaz García, F., Rubio Pascual, F.J., Abati, J., Marquínez, J., 1996. Variscan exhumation of a subducted Paleozoic continental margin: the basal units of the Ordenes Complex, Galicia, NW Spain. Tectonics 15 (1), 106–121.

Narr, W., Suppe, J., 1991. Joint spacing in sedimentary rocks. Journal of Structural Geology 13, 1037–1048.

Nedham, T., Yielding, G., Fox, R., 1996. Fault population description and prediction using examples from the offshore UK. Journal of Structural Geology 18, 155–167.

Pannatier, Y., 1996. VARIOWIN 2.2.: Software for Spatial Data Analysis in 2D. Springer-Verlag, New York.

Pebesma, E.J., Wesseling, C.G., 1998. GSTAT, a program for geostatistical modelling, prediction and simulation. Computers & Geosciences 24, 17–31.

Pérez Estaún, A., Martínez Catalán, J.R., Bastida, F., 1991. Crustal thickening and deformation sequence in the footwall to the suture of the Variscan belt of Northwest Spain. Tectonophysics 191, 243–253.

Proyecto ZOA, 1996. Memoria Cartografía Geológica y Estructural. Rocas Plutónicas, Albalá (G111). Enresa (94-G111-IF), Madrid, Vol. II, 249pp.

Reguilón, R.M., 1988. Las mineralizaciones de uranio y fósforo de los granitos de Trujillo, Plasenzuela, Albalá, Montánchez y Alburquerque. Ph.D. thesis, Univ. de Salamanca, 276pp.

Reguilón, R., Arribas, A., Martín-Izard, A., Mangas, J., 1996. Las mineralizaciones de U de la Carretona y Casa del Gallo en el granito de Albalá (Cáceres). Geogaceta 20 (7), 1598–1600.

Sanderson, D.J., Roberts, S.P., McGowan, J., Gumiel, P., 1991. Hercynian transpresive tectonics at the southern margin of the Central-Iberian Zone, West Spain. Journal Geological Society of London 148, 889–893.

Scholz, C.H., Anders, M.H., 1994. The permeability of faults. In: The Mechanical Involvement of Fluids in Faulting. US Geol. Survey. Open-File Repport 94-228, pp. 247–253.

Schulz, S.E., Evans, J.P., 1998. Spatial variability in microscopic deformation and compositions of the Punchbowl fault, southern California: implications for mechanisms, fluid-rock interaction, and fault morphology. Tectonophysics 295, 223–244.

Schulz, S.E., Evans, J.P., 2000. Mesoscopic structure of the Punchbowl Fault, Southern California and the geologic and geophysical structure of active strike-slip faults. Journal of Structural Geology 22, 913–930.

Sibson, R.H., 1977. Fault rocks and fault mechanisms. Journal Geological Society London 133, 191–213.

Villaescusa, E., Brown, E.T., 1990. Characterizing joint spacial correlation using geostatistical methods. In: Barton, N., Stephansson, O. (Eds.). Rock Joints. Balkema, Rotterdam, pp. 115–122.